1991-08-15

Statistical properties of nearsurface flow in the California coastal transition zone

Brink, K.H.; Beardsley, R.C.; Niiler, P.P.; Abbott, M.; Huyer, A.; Ramp, S.; Stanton, T.; Stuart, D.

American Geophysical Union.

Brink, K. H., et al. "Statistical properties of nearsurface flow in the California coastal transition zone." Journal of Geophysical Research: Oceans 96.C8 (1991): 14693-14706. http://hdl.handle.net/10945/70991

JOURNAL OF GEOPHYSICAL RESEARCH, VOL. 96, NO. C8, PAGES 14,693–14,706, AUGUST 15, 1991

Statistical Properties of Near-Surface Flow in the California Coastal Transition Zone

K. H. BRINK,[1] R. C. BEARDSLEY,[1] P. P. NIILER,[2] M. ABBOTT,[3] A. HUYER,[3] S. RAMP,[4] T. STANTON,[4] AND D. STUART[5]

During the summers of 1987 and 1988, 77 near-surface satellite-tracked drifters were deployed in or near cold filaments near Point Arena, California (39°N), and tracked for up to 6 months as part of the Coastal Transition Zone (CTZ) program. The drifters had large drogues centered at 15 m, and the resulting drifter trajectory data set has been analyzed in terms of its Eulerian and Lagrangian statistics. The CTZ drifter results show that the California Current can be characterized in summer and fall as a meandering coherent jet which on average flows southward to at least 30°N, the southern end of the study domain. From 39°N south to about 33°N, the typical core velocities are of $O(50\ \mathrm{cm\ s^{-1}})$ and the current meanders have alongshore wavelengths of $O(300\ \mathrm{km})$ and onshore-offshore amplitude of $O(100\text{–}200\ \mathrm{km})$. The lateral movement of this jet leads to large eddy kinetic energies and large eddy diffusivities, especially north of 36°N. The initial onshore-offshore component of diffusivity is always greater than the alongshore component in the study domain, but at the southern end, the eddy diffusivity is more isotropic, with scalar single particle diffusivity $(K^{xx} + K^{yy})$ of $O(8 \times 10^7\ \mathrm{cm^2\ s^{-1}})$. The eddy diffusivity increases with increasing eddy energy. Finally, a simple volume budget for the 1988 filament observed near 37°N off Point Arena suggests that subduction can occur in a filament at an average rate of $O(10\ \mathrm{m\ d^{-1}})$ some 200 km offshore, thus allowing the cold water initially in the filament core to sink below the warmer ambient water by the time the surface velocity core has turned back onshore. This process explains why satellite temperature and color imagery tend to "see" only flow proceeding offshore.

1. INTRODUCTION

One central goal of the Coastal Transition Zone (CTZ) program has been to understand the filaments of cold water which project offshore from the coast of northern California during the summer upwelling season. To help achieve this goal, intensive physical oceanographic measurements were made in the upper ocean off California in the summers of 1987 and 1988 to provide new and more complete descriptions of the water property and velocity structure of these cold filaments and their surrounding environment. Based in part on the successful early exploration into the nature of filaments by *Davis* [1985*a*] using radio-tracked surface drifters, the CTZ field program included a large satellite-tracked drifter program to observe and characterize the near-surface flow and its dynamical properties. Since the filaments were known to be surface-intensified features, the CTZ drifters were all drogued at a common depth of 15 m, which frequently placed the drogue within the surface mixed layer.

The objective of this study is to use the CTZ drifter measurements to characterize statistically the kinematics and dynamics of the near-surface (15 m) flow. Since drifters tend to spread out over a broad area with time, making full use of the drifter data base often implies looking on a much broader spatial scale than that encompassed by the rest of the CTZ measurements, which were confined to the area north of roughly 37°N (Figure 1). The drifter data used here cover latitudes from about 30° to 39°N, that is to say, most of the coast of California. Such broad scale descriptions will sometimes tend to deemphasize specific filamentary features, although these are of considerable interest. A description of the individual CTZ drifter trajectories, including the tendency for the near-surface (15 m) flow to proceed offshore along the axis of a cold filaments, is presented by M. Swenson et al. (Drifter observations of the dynamical and thermodynamical structures in a cold filament off Point Arena, California, in July 1988, submitted to *Journal of Geophysical Research*, 1990, hereinafter referred to as Swenson et al., 1990).

The following results deal with a number of specific topics, all addressed statistically. First, the "Eulerian" mean flow and its accompanying variability will be treated. Next, the dispersion properties measured using the drifters will be discussed. Both of these first two topics tend to deal with the broader spatial scales. Next, the momentum balance for near-surface flow will be treated in the CTZ intensive area. Finally, the relation of drifter kinematics to frontal locations in the Point Arena vicinity will be considered.

2. THE OBSERVATIONAL BASE

The primary measurement system is the Tristar Mark II drifter [*Niiler et al.*, 1987]. These instruments have large (6 m) radar reflector-shaped drogues located at a central depth of 15 m. The drogue and surface float design has been calibrated by in situ current measurements and follows horizontal currents to within about 1 cm/s under conditions representative of those encountered here. The drifters are tracked using the Argos satellite system. Typically, eight fixes per day were obtained during the CTZ program, and

[1]Woods Hole Oceanographic Institution, Woods Hole, Massachusetts.
[2]Scripps Institution of Oceanography, La Jolla, California.
[3]College of Oceanography, Oregon State University, Corvallis.
[4]Department of Oceanography, Naval Postgraduate School, Monterey, California.
[5]Department of Meteorology, Florida State University, Tallahassee.

Paper number 91JC01072.
0148-0227/91/91JC-01072$05.00

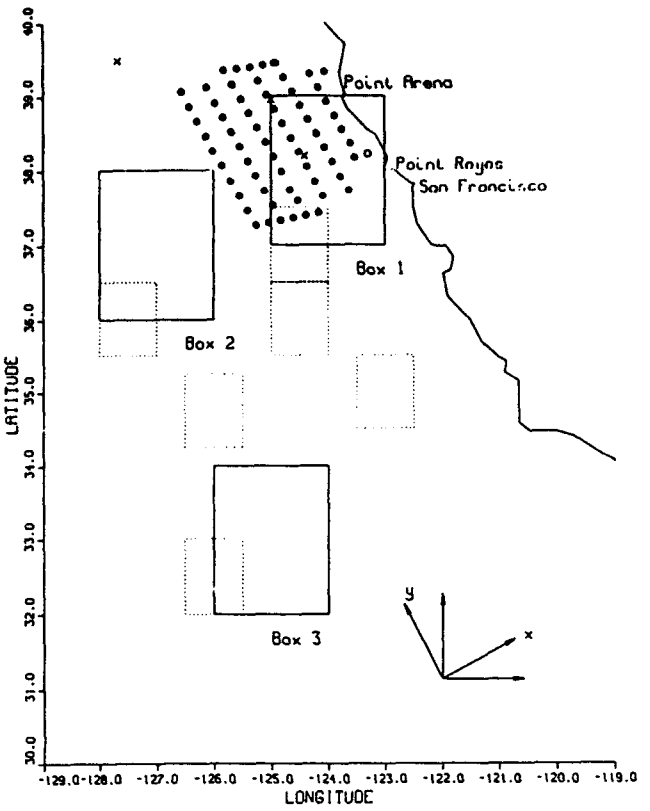

Fig. 1. Locator map. The open circle denotes the location of NDBC buoy 46013. The solid circles are locations of hydrographic stations for a typical 1988 survey, defining the CTZ intensive region. Boxes represent the areas within which diffusivities and Lagrangian time scales were computed. Crosses represent the locations of the *Stabeno and Smith* [1987] moorings used to estimate Eulerian time scales.

the accuracy per fix is generally about 300 m. After initial editing of the drifter positions, cubic splines (each 4 days in length) are used to smooth the tracks and remove inertial and tidal variance. The splines effectively represent a low-pass filter with a half power point of about 0.45 cpd.

The drifters were deployed during the late spring or summer of 1987 and 1988 in small coherent clusters. Most of the 25 deployments in 1987 were in May and June, while most of the 52 in 1988 were in July or early August. In 1987 the drifters provided good data for typically 25 days, while in 1988, good data were typically available for 6 months or more following launch. The drifters were usually launched in clusters of 3–17, with separations of 5–20 km from nearest neighbors. Smaller separations were used in larger deployments. The deployment strategy was intended to allow mapping of velocity and relative vorticity within the Point Arena filament (Swenson et al., 1990). The total set of drifter tracks (Figure 2) gives a measure of the amount of data available.

In addition to the drifter trajectories, several other sources of data were employed. Conductivity-temperature-depth (CTD) surveys were made repeatedly on a regular grid (Figure 1) in the CTZ intensive area. Details on the hydrographic observations are given by *Fleischbein et al.* [1989] and *Huyer et al.* [this issue]. Winds were measured at 10 m elevation at NOAA Data Buoy Center (NDBC) environmental buoy 46013, located at 38°13′N, 123°18′W. The wind

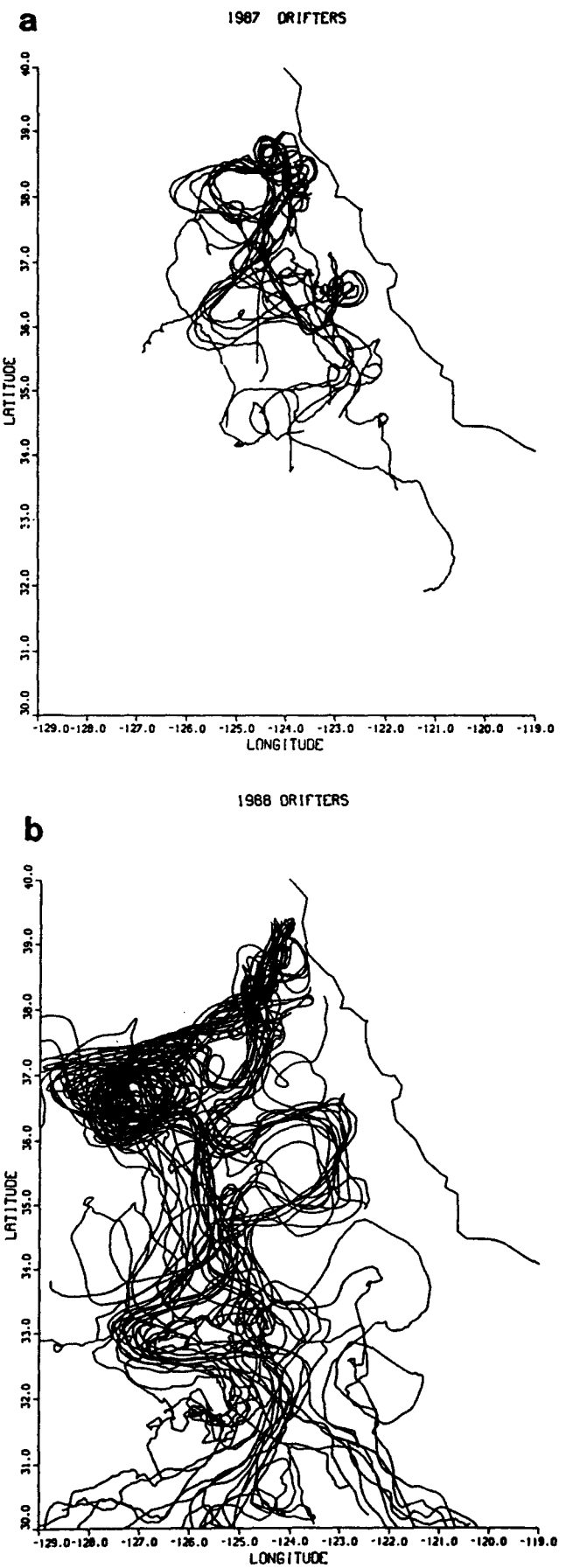

Fig. 2. Complete (*a*) 1987 and (*b*) 1988 CTZ drifter tracks.

velocity time series were converted into wind stresses using the method of *Large and Pond* [1981], and then spline-fit in the same way as the drifter positions to provide a low-pass-filtered wind stress time series. Finally, advanced very high resolution radiometer (AVHRR) images of surface temperature were used. These were calibrated and registered using the techniques described by *Kelly and Davis* [1986], except that no view angle correction was made.

3. EULERIAN STATISTICS

The general properties of the near-surface flow will first be described in terms of "Eulerian" flow patterns. We use the term "Eulerian" cautiously because of the bias introduced by the tendency for drifters to avoid divergences and to enter an area only when the flow is in the right sense. In order to make these estimates, 1-day averages of smoothed drifter velocities were sorted into 0.5° by 0.5° latitude-longitude bins. Bins containing less than 10 drifter days of data were deleted from further consideration. For each bin, the vector mean flow and the standard deviations along principal axes directions were computed. The results are shown in Figure 3 for 1987 and 1988 separately.

In the bins where there was a large data base (greater than 50 drifter days), standard deviations of currents were

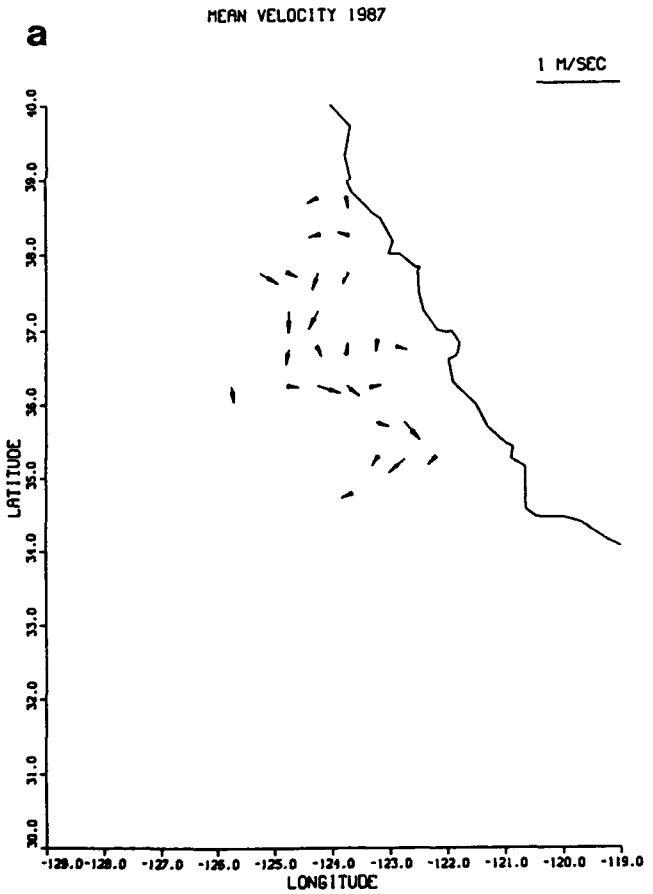

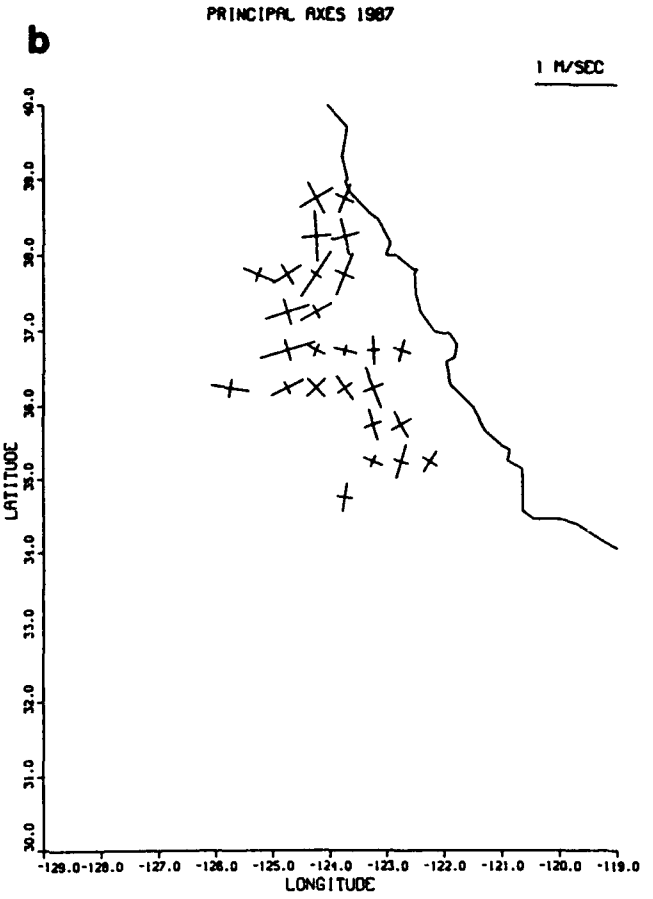

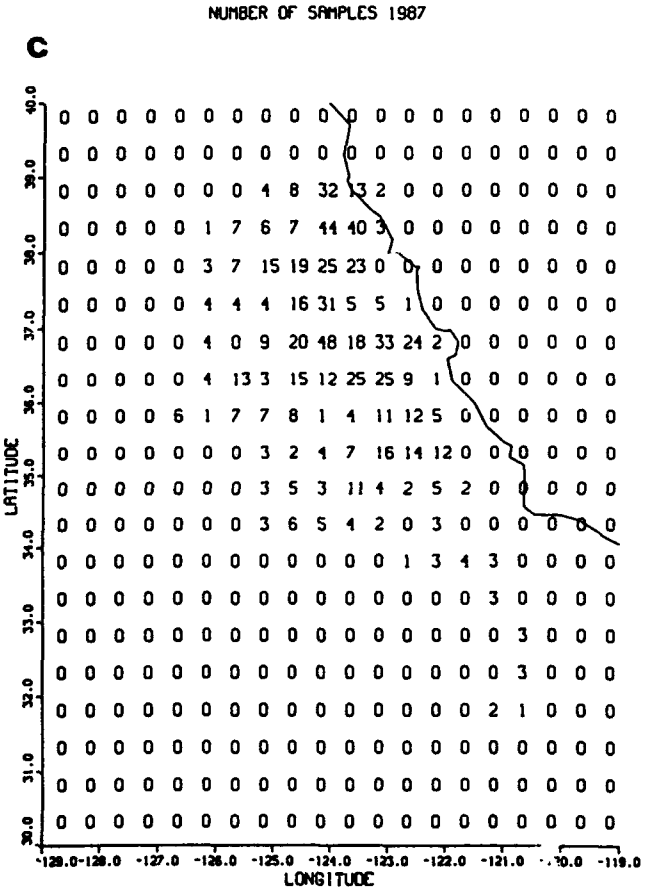

Fig. 3. Eulerian statistics from drifters. Results are only shown for boxes with more than 10 drifter days of data. Dots represent box centers. (*a*) Mean velocity for 1987. (*b*) Standard deviations in principal axis system for 1987. The half-length of each cross represents 1 standard deviation. (*c*) Number of drifter days per box for 1987. (*d*) Mean velocity for 1988. (*e*) Standard deviations in principal axis system for 1988. (*f*) Number of drifter days per box for 1988.

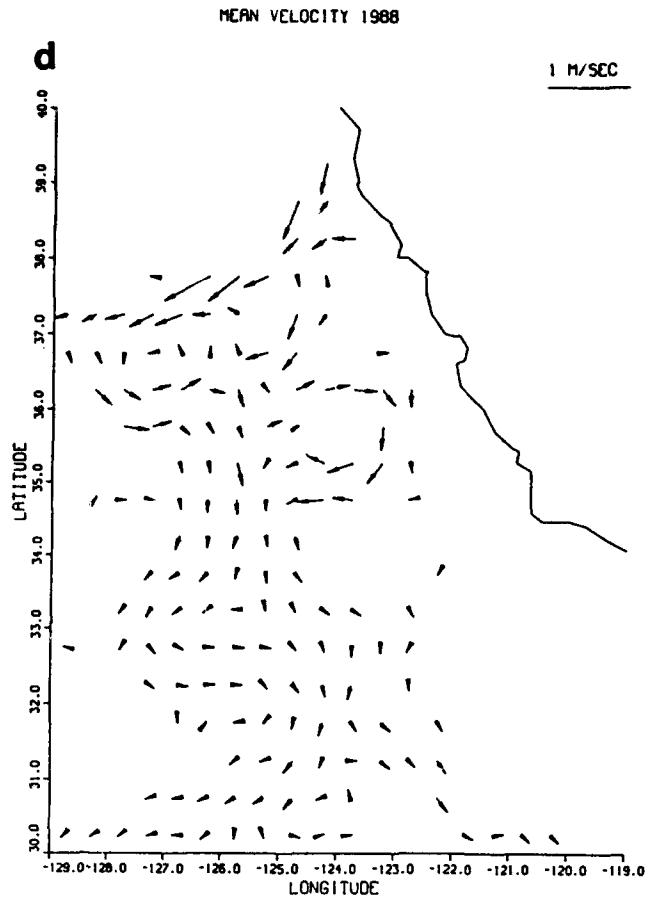

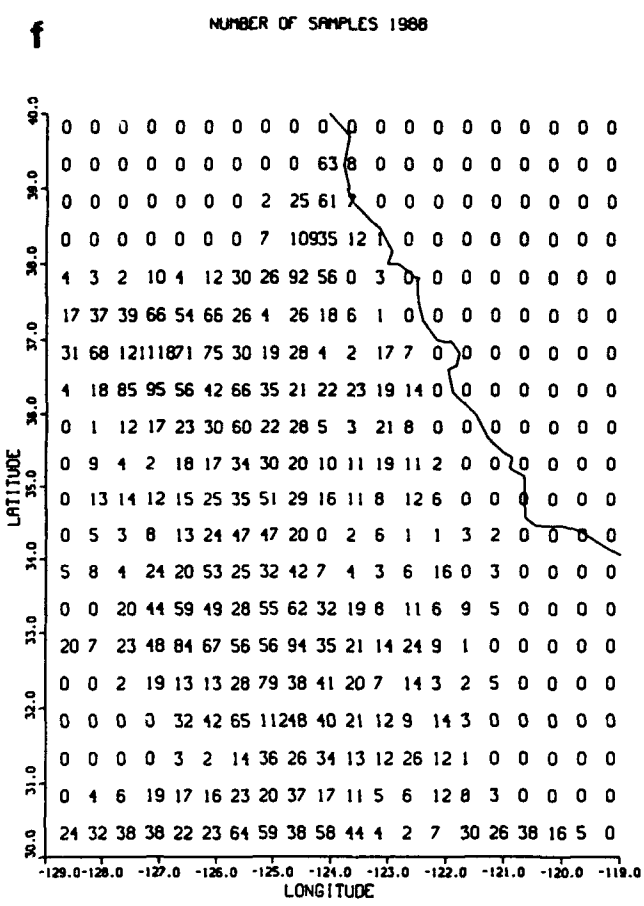

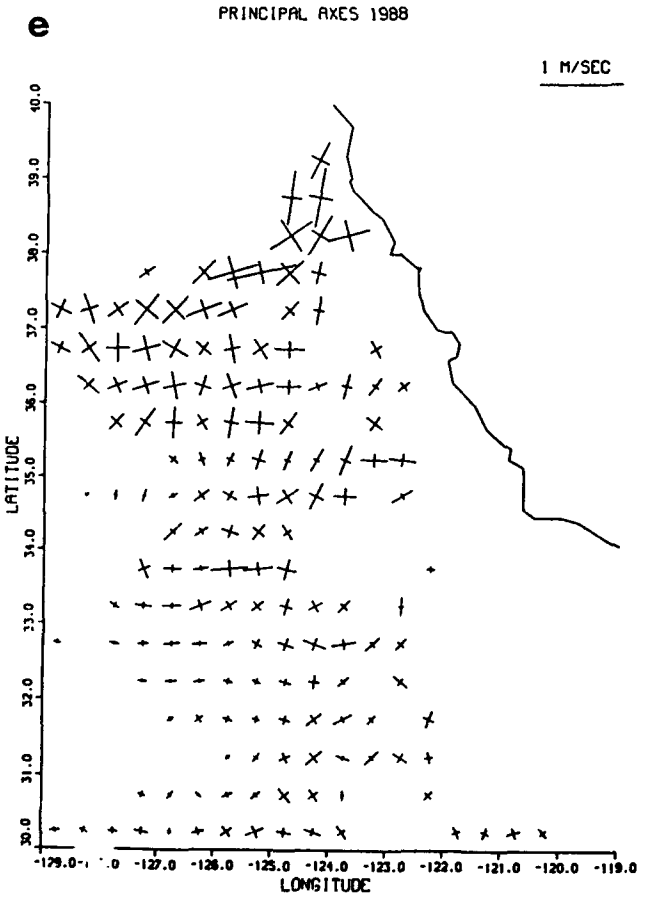

typically about 20–30 cm s^{-1}. The Eulerian independence time scale was calculated from moored current meter records in the region (Figure 1) at depths of 145–200 m [*Stabeno and Smith*, 1987]. Although these instruments are far from the surface, they are the shallowest long records available. Although currents in the region are definitely baroclinic, reversals of direction in the upper 200 m generally occur only when near-surface currents are weak ($\lesssim$10 cm s^{-1}), [e.g., *Kosro et al.*, this issue], so we believe that the 145–200 m Eulerian current independent time scales are at least representative of the near-surface flow. The average value obtained from these records was 12 days (obtained by integrating the autocorrelation over only positive lags [e.g., *Kundu and Allen*, 1976]. The drifter bins with the best data coverage span about 100 calendar days, or represent about 4 degrees of freedom using the current meter time scale. Thus the 90% error bounds on velocity in the most data-rich bins are typically about $\pm$26 cm s^{-1} (about 1.5 times the length of an arrowhead in Figure 3). The most data-rich bins (Figures 3*c* and 3*f*) tend to be those along the core of the mean jets visible in Figure 3. Note that in a sense, this is a conservative error estimate, since it is based on calendar days of occupation rather than drifter days in a box.

The means from both years (Figure 3) and from the two years combined (Figure 4) show a meandering core current which, on the whole, proceeds southward. Note that, despite similar release points, the 1987 and 1988 data sets have very different spatial coverages, with the 1987 drifters being more concentrated inshore. In both years, the average core velocities are about 50 cm s^{-1}, and the meandering

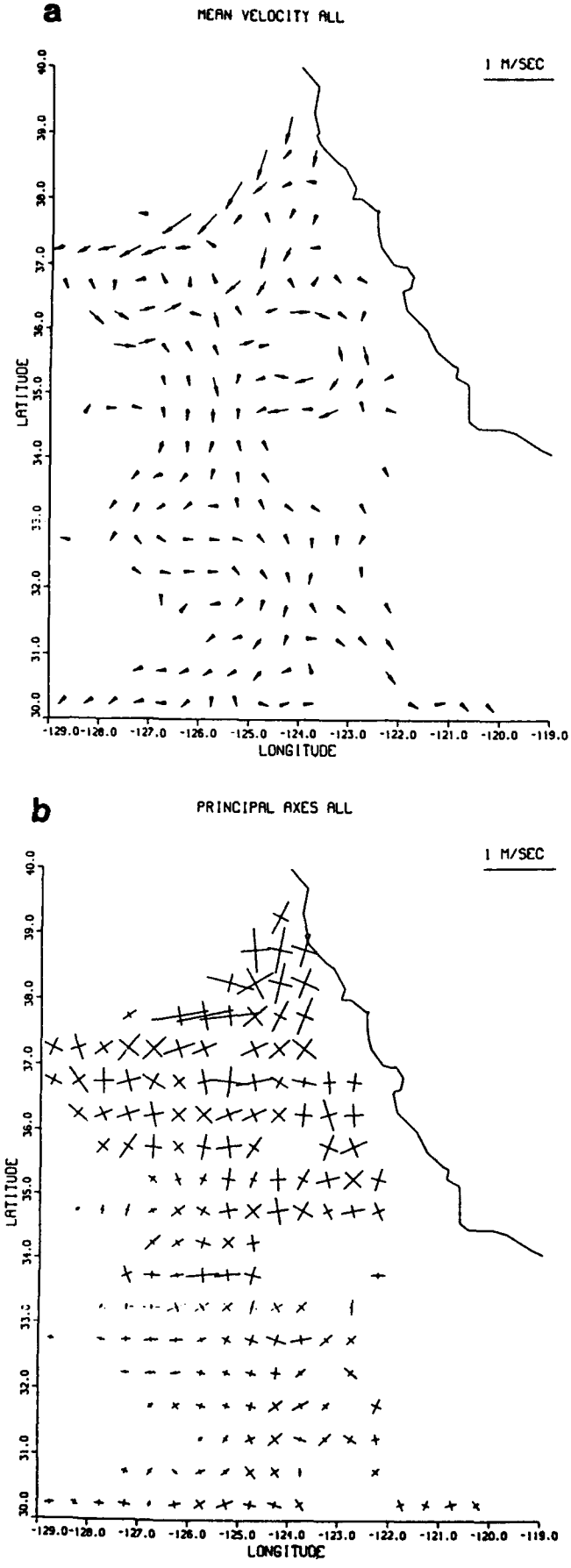

Fig. 4. As in Figure 3, but based on the merged 1987 and 1988 data sets. (a) Mean velocity. (b) Standard deviations.

patterns have alongshore wavelengths of $O(300$ km). The locations of the cores differ south of about 36.5°N between the two years, and the differences are reflected in data distributions which barely overlap south of 35°N. For this reason, only in the area north of about 36°N can the 1987 and 1988 data be compared meaningfully. In 1987, the offshore-directed branch near 37°N does not proceed as far offshore as the similar feature near 37.5°N in 1988. This is qualitatively consistent with AVHRR images, which suggest that the filaments were shorter in 1987 than in 1988. Both years show significant eastward velocity at about 36°N, suggesting that at least this part of the meander field may be geographically stable. It is possible that the differences between the 1987 and 1988 mean current fields are related primarily to seasonal variability associated with the slightly earlier 1987 launches. Considerable caution, of course, must be used in interpreting the mean flow results because the Eulerian sampling grid is dependent upon the flow itself and the specific, tightly clustered deployment scheme used in the CTZ program. A further complicating factor is that, while the drifters were deployed in May–August, most of the fixes in the southern region were obtained in November and December. Thus there is a possibility that seasonal variations in the California Current system can be aliased into apparent spatial variations of the mean flow. Climatological 0/500 dbar flow patterns in this area are oriented northwest–southeast [*Hickey*, 1979]. In the summer, flow is southeastward everywhere, while in the winter, flow within 100–200 km of shore reverses to flow northwestward. In both seasons, maximum mean alongshore velocities are about 15 cm s^{-1}, and 5 cm s^{-1} is typical. Thus a seasonal aliasing of our mean flow seems possible, since the climatological "California Current" as defined by the *0/500* dbar dynamic topography [*Hickey*, 1979] is indeed weaker in the winter, although the combined mean drifter flow (Figure 4) is both stronger and directed more southward than the climatological version [*Hickey*, 1979] over the entire domain.

The standard deviations of velocity present a rich pattern. Perhaps the most obvious aspect is a tendency for variance to decrease from north to south (Figure 4). This could reflect a true north–south gradient of the eddy kinetic energy, seasonal variations in velocity variance or it could represent a tendency for more evenly spread velocity sampling farther to the south, since most of the drifters were deployed in or near energetic structures near 38°–39°N. A further tendency is for the major axis of variability to line up loosely with the mean flow in the jet core regions, most notably in the northern part of the domain. South of about 33°N, where the mean jet is no longer very pronounced, the principal axis orientations appear to be fairly random, although there is a tendency for the axes to tilt toward the jet core, suggesting a convergence of southward momentum. The tendency for current variability to decrease toward the south could represent seasonal variability if currents were to become weaker in the winter. This does not appear likely, though, since *Poulain and Niiler* [1989] found relatively small eddy kinetic energies, representing all seasons, of about 110 cm^2 s^{-2} in the area south of 34°N. This is consistent with a real southward decrease in current variability. It therefore seems likely that the trend of lower energy toward the south is primarily geographical, rather than seasonal.

All told, the Eulerian statistics confirm the highly variable nature of the California Current system. The core jet

locations differed considerably between 1987 and 1988. Further, in most cases, the standard deviation of currents is greater in magnitude than the mean. This, of course, implies that an Eulerian mean California Current will look very little like an instantaneous realization. It is thus interesting to ask whether the California Current has a sharp, meandering high-velocity core throughout the entire north–south extent of the domain. This is clearly the case north of 36°N, but the weaker means and fluctuations toward the south could be due either to the core becoming diffuse and weak, or to meandering over a broad region of otherwise weak variability. In order to gain some further insight about this point, we found the strongest individual velocity measurement in each 0.5° box (Figure 5). Large velocities are found at all latitudes, so the meandering jet model seems to apply throughout. There is, however, a tendency for the peak velocities to be about 20% weaker south of 33°N than north of that latitude. This north–south decrease in core velocities coincides roughly with the location where both the mean and fluctuating currents (Figure 4) become noticeably weaker, and Geosat estimates of sea surface height variability decrease sharply [*Flament et al.*, 1989]. Thus, we envision the California Current as a meandering but coherent jet over the domain of study, with a core velocity maximum which decreases south of about 33°N. The kinematic implication of this is that the core spreads out into a somewhat broader, less energetic flow as the current proceeds southward.

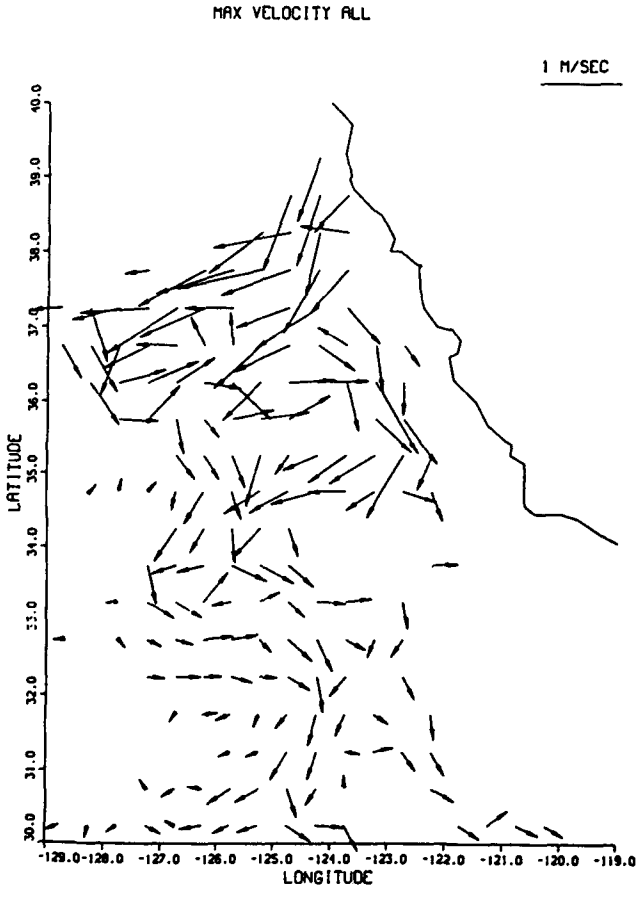

Fig. 5. Velocity corresponding to the maximum speed observed in each 0.5° box (total data set).

4. EDDY DIFFUSIVITIES

4.1. Single Particle Statistics

Single particle dispersion statistics were computed in the same manner used by *Davis* [1985*b*]. These measure the tendency for an individual water parcel to deviate from the ensemble average trajectory. Specifically, the eddy diffusivity is defined as

$$K^{nm}(\vec{x}) = \frac{1}{2}\frac{d}{dt}\mu^{nm}(\vec{x},t), \qquad (1a)$$

where

$$\mu^{nm}(\vec{x},t) = \frac{1}{N}\sum r^{n'}(\vec{x},t)r^{m'}(\vec{x},t), \qquad (1b)$$

where n and m can be either x or y, $r^n(\vec{x},t)$ is the location of a drifter in the n direction (since the time of its launch at $t=0$ at position $\vec{x}$), and $r^{n'}$ is the difference in the n direction between an individual drifter's location and the mean drift, $r^{n'} = r^n - (1/N)\sum r^n$. The average is over all N drifters which appear within a particular box. Since the memory of drifters tends to be short (2–6 days; see section 5), all drifters were treated as newly deployed after 10 days if they remained in the box. That is to say that, for the purpose of calculating μ^{nm}, a single drifter could yield several trajectories, each starting 10 days after the other if the drifter was in the box at its new starting time. This is simply a means of retrieving more information from the available data, e.g., *Poulain and Niiler* [1989]. For all diffusivity calculations, the coordinate system is rotated 28° counterclockwise so that x is perpendicular to the general trend of the California coastline between 34°30′N and 39°N (Figure 1). This had the effect of decreasing the off-diagonal elements of the dispersion tensor K^{xy} in some cases, while not increasing it substantially for locations farther from the coast.

The single point dispersion calculations were carried out for three boxes having particularly good data coverage (Figure 1). The first box includes the filaments within which most drifters were deployed. The second box is farther offshore and includes the region in which most 1988 drifters cease going offshore. The third box lies in the southern region where the drifters tend to be well dispersed. The results for the merged (1987 and 1988) measurements are shown in Figure 6. In all cases, the xx (onshore-offshore) diffusivity is the largest component during the first 4 days. For the two northern boxes, however, the diffusivity decreases by day 5 and then passes through zero. This behavior may reflect the influence of long-lasting flow structures (e.g., the filament). For the southernmost box, no such persistent flow structures were apparent and the xx diffusivity had more of a tendency to increase monotonically with time, as expected in a turbulent field [e.g., *Davis*, 1985*b*].

In all cases, the initial alongshore yy diffusivity tended to increase with time, and not pass through zero. This suggests that the flow structures complicating the xx dispersion act mainly in the onshore-offshore direction, as might be expected for meanders oriented roughly perpendicular to the coast. The off-diagonal diffusivity was small for $t < 10$ days but was of the same magnitude as the alongshore component of diffusivity.

The results of the single point diffusivity calculations are

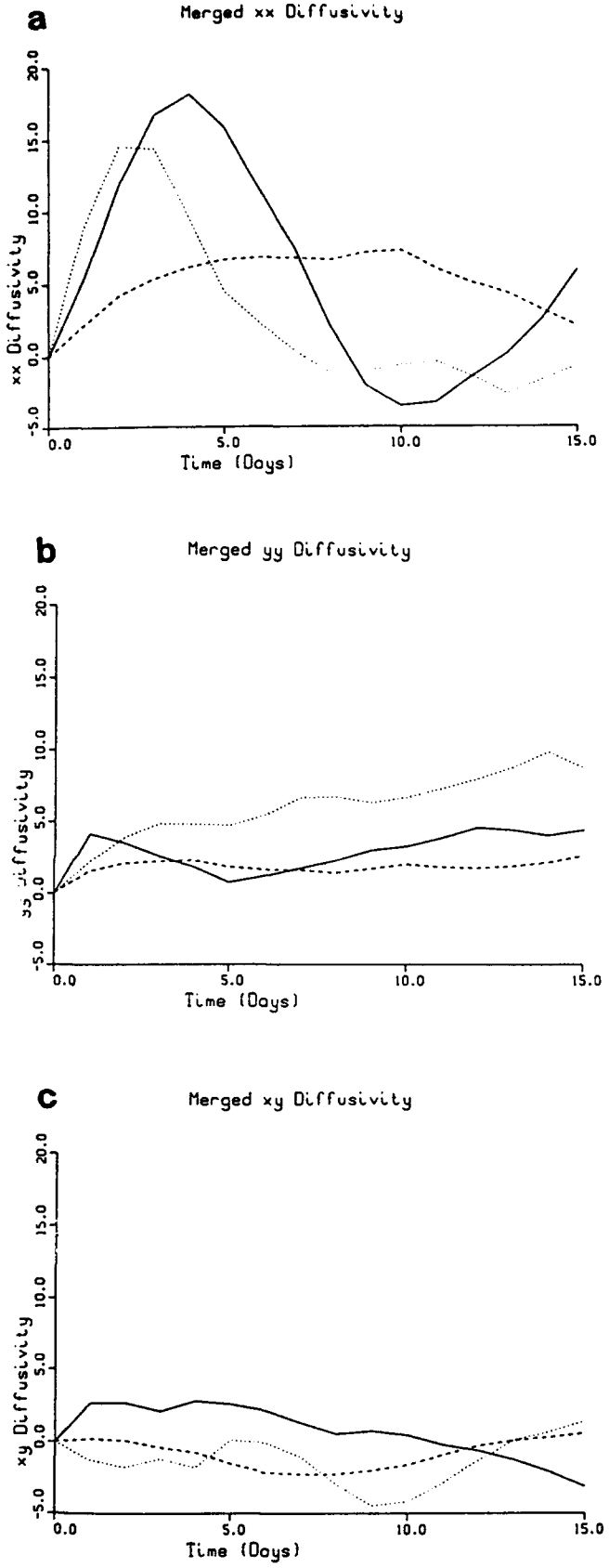

Fig. 6. Single point diffusivities, calculated with the merged (1987 and 1988) data sets. Solid line, box 1; dotted line, box 2; dashed line, box 3. All diffusivity values are divided by $10^7 \mathrm{cm}^2\ \mathrm{s}^{-1}$. (*a*) Onshore-offshore (xx) component. (*b*) Alongshore (yy) component. (*c*) Off-diagonal (xy) component.

summarized (Table 1) in terms of the average values over the first 10 days. Except for the relatively sparse data base in 1987 (±40%), the 95% confidence intervals on the 10-day-averaged diffusivities are typically ±20%. The meaning of traditional confidence intervals in this situation is a bit problematic, especially in box 1, since the drifters are not obviously statistically independent. This follows because they are all launched into an energetic flow feature which was long-lived relative to drifter transit times of 5–10 days [e.g., *Kosro et al.*, this issue]. Because the drifters are all sampling the same feature with a short (1–2 months) time window, it seems likely that individual drifters are not statistically independent and that the means and diffusivities do not truly reflect an ideal "ensemble."

It is worthwhile to ask whether the diffusivity can be parameterized simply in terms of the eddy kinetic energy of the system,

$$E'_K = \frac{1}{2}\frac{1}{N}\sum|\vec{v} - \bar{\vec{v}}|^2,$$

where $\bar{\vec{v}}$ is the vector average velocity within a box. Note that since this measure accounts for deviations from both the spatial and temporal mean, it will tend to be larger than the eddy kinetic energy computed at a single site from, say, a current meter mooring (since the single point variance is computed relative to a temporal mean only). In order to reduce scatter, a "scalar diffusivity"

$$K = K^{xx} + K^{yy}$$

averaged over 10 days lag is compared with E'_K (Figure 7). The open circles correspond to values calculated in the larger boxes, while the dots correspond to estimates made in smaller boxes (dashed boxes in Figure 1). The result suggests a dependence of K on E'_K of the form

$$K = b(E'_K)^{1/2},$$

where $b = 42$ km (by least squares fit). This result suggests [*Krauss and Böning*, 1987] that there is a constant eddy length scale, but that the Lagrangian time scale is not constant, a finding consistent with our time scale calculations (see below and Table 1). Our isotropic mixing length of 42 km can be compared to *Krauss and Böning's* [1987] range of 31–39 km for the North Atlantic Ocean (using their definition). Such comparable values suggest that our measurements correspond to an open-ocean regime, not influenced by boundary effects in a gross sense.

The averaged single point diffusivity is always initially largest (for short time lags) in the onshore-offshore direction (the exception being in 1987 when the current meanders were less pronounced). To interpret this result, K^{nm} can be thought of as the diffusivity to be used in a steady state diffusive-advective model. The net flow is southward (or toward negative y) in general (Figure 4), while the onshore-offshore component shows substantial variability but little net trend. Thus advection moves the drifters fairly consistently toward the south, while the "diffusion" (parameterizing the various onshore and offshore flow patterns) leads mainly to a spreading in the onshore-offshore direction.

4.2. *Taylor's Hypothesis*

If the flow field is homogeneous and stationary within a box, then by Taylor's hypothesis the eddy diffusivity is identically equal to

TABLE 1. Eddy Diffusivities and Independence Time Scales

Year	Box	n^*_{max}	10-Day Average Single Point Diffusivities, $cm^2\ s^{-1} \times 10^{-7}$ K_{xx}	K_{yy}	K_{xy}	Kinetic Energy, $cm^2\ s^{-2}$ Mean	Eddy	Independence Time Scales,† days T_L^x	T_L^y
1987	1	43	3.25	1.88	1.05	114	341	2.1	1.8
1988	1	83	10.04	2.66	2.32	381	811	4.2(2.8)	0.9
	2	175	5.45	4.95	-1.66	56	719	2.5(1.0)	1.7(1.7)
	3	329	5.61	1.77	-1.21	100	228	5.8(3.3)	2.7
Merged	1	126	8.62	2.43	1.87	227	714	3.3(2.8)	0.9(0.8)
	2	181	5.34	4.95	-1.57	54	718	2.5(1.0)	1.8(1.6)
	3	329	5.61	1.77	-1.21	100	228	5.8(3.3)	2.7

* Maximum number of drifter days in the calculation.
† From (3) and (6). Values in parentheses are time scales integrated to 50 days. Such values are only given if the result stabilized for the last 20 days. Values not in parentheses are for integrations terminated at the first zero crossing of the autocorrelation function.

$$K^{nm} = \overline{u^{n'}u^{m'}} \int_0^t L^{nm}(t')dt', \qquad (2)$$

where L^{nm} is the lagged correlation function of the Lagrangian n and m components of flow (u^n, u^m), and $\overline{u^{n'}u^{m'}}$ is the zero lag covariance. The Lagrangian correlation function L^{nm} was computed as

$$L^{nm}(t') = \left[N\sigma^n(0)\sigma^m(t')\right]^{-1} \sum^N u^{n'}(0)u^{m'}(t'), \qquad (3)$$

where the standard deviations σ^n are recomputed separately for each time lag because the Lagrangian mean changes with lag, a finding consistent with *Davis* [1985*b*]. The sum is over all N drifter trajectories originating in the box. Here we calculate the right-hand side of (2) for each of the three boxes. Note that using this form of the autocorrelation function, which is necessary to account for the inhomogeneity of the flow, means that the results of (1) and (2) need not be identical. Thus the extent to which this estimate agrees with the K^{nm} estimated using (1) is a measure of the homogeneity of the flow.

Comparisons of the two estimates of diffusivity for boxes 1 and 3 are shown in Figures 8. Generally, the two estimates agree well for the first day after drifter launch, but substantial differences occur within 5 days. The divergence can be understood through examination of velocity covariance as a function of time since launch. The cases where the two estimates diverge quickly correspond to cases where the covariances (e.g., kinetic energy) change rapidly as a function of time since launch. That is, divergence of the estimates corresponds to cases of strongly inhomogeneous flow statistics over scales comparable to, or smaller than, the box size. The cases where the two estimates diverge slowly, on the other hand, correspond to situations where the flow statistics remain relatively constant with time after launch. It is worth noting, too, that in box 3, Taylor's hypothesis works fairly well, and this is a region of relatively uniform Eulerian statistical properties (Figure 4).

Taken together, the tests of Taylor's hypothesis lead to the conclusion that the flow in the region sampled off California is rather inhomogeneous on scales as small as 200 km. This should perhaps not be surprising given the presence of a coast and the apparent north–south variation in Eulerian statistics.

4.3. Particle Pair Dispersion

The rate at which two particles separate is the appropriate eddy diffusivity to consider when examining the time-dependent behavior of a system [*Davis*, 1985*b*]. This particle pair diffusivity is defined by

$$\alpha^{nm} = \frac{1}{4}\frac{d}{dt}\nu^{nm}, \qquad (4a)$$

where

$$\nu^{nm} = \frac{1}{N}\sum s^{n'}s^{m'}. \qquad (4b)$$

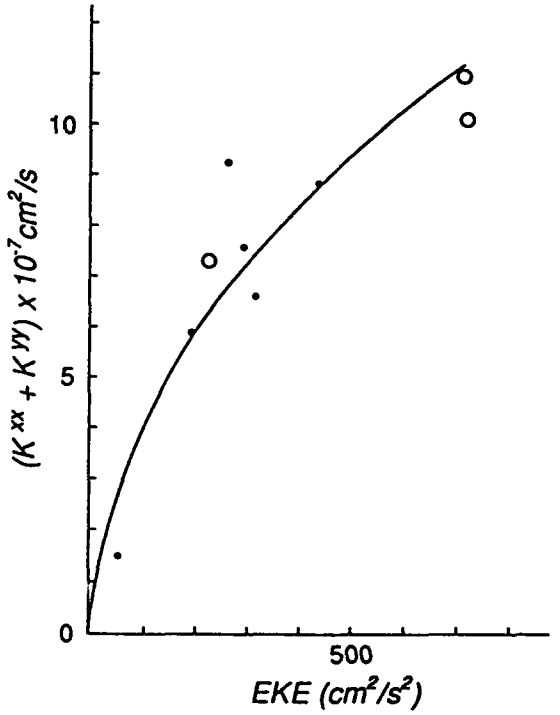

Fig. 7. "Scalar diffusivity" as a function of eddy kinetic energy. Circles indicate large box estimates (solid boxes in Figure 1). Dots indicate small box estimates (dashed boxes in Figure 1).

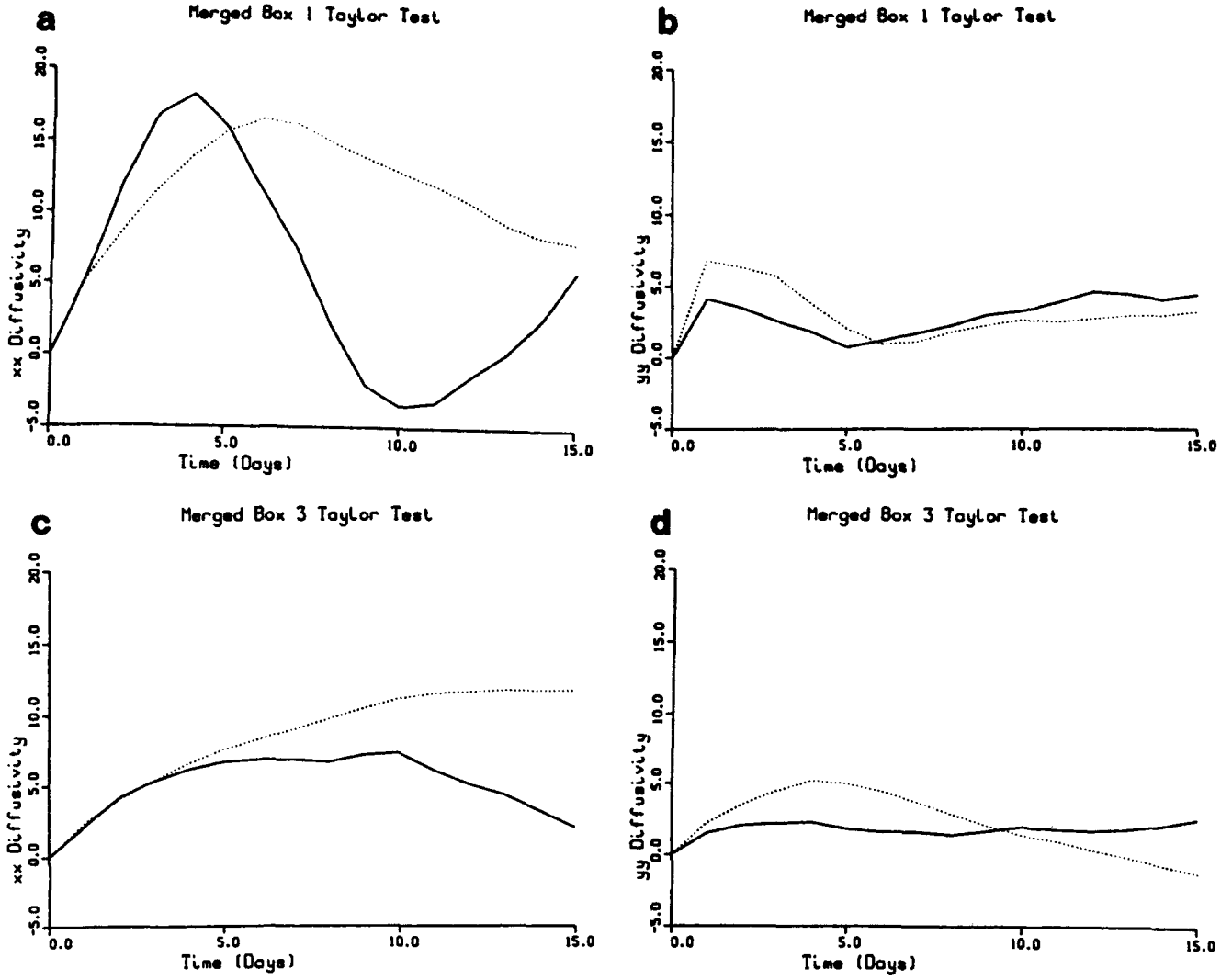

Fig. 8. Comparisons of single point diffusivities computed directly (solid line) and using Taylor's hypothesis (dotted line). All diffusivity values are divided by $10^7 cm^2 s^{-1}$. (*a*) Onshore-offshore (xx) component, box 1. (*b*) Alongshore (yy) component, box 1. (*c*) Onshore-offshore (xx) component, box 3. (*d*) Alongshore (yy) component, box 3.

The n component of separation between two drifters is s^n, and $s^{n'}$ is the deviation of a given drifter pair from that of the mean at that time step. The average is over all drifter pairs, with no geographical binning. Following *Davis* [1985*b*], the calculation of ν^{nm} was binned by the initial separation distance between drifters. No attempt was made to carry out separate calculations for different geographical areas due to the need to accumulate large numbers of degrees of freedom, although nearly all pairs started in either box 1 or 2 (Figure 1). As in the single particle dispersion calculations, all drifters were treated as newly launched after 10 days. The bins corresponded to initial separations of less than 16 km, between 16 and 32 km, and between 32 and 64 km.

The results of the calculations for the merged 1987–1989 data set, displayed as a function of pair separation (which increases with time for the results given) are shown in Figure 9. The initial separation bin can be identified by the location where a given curve passes through $\alpha = 0$. As in the case of single particle diffusivities, the onshore-offshore xx dispersion is the largest, yielding values substantially larger (for the same separation) than those reported by *Davis* [1985*b*] for the nearshore region near 38°N. The alongshore diffusivities are far smaller than the onshore-offshore component, apparently as a result of the alongshore flow component tending always to have an equatorward component, as would be found in a meandering jet. The off-diagonal components of pair dispersion also tend to be small and show little net pattern. In all cases, the dispersion values tend to decrease toward zero, corresponding to a state where particle pair separations become relatively constant, at least for a time. The pair diffusivities tend to be the same magnitude as the single particle dispersions, although pair yy values tend to be somewhat smaller than single particle yy dispersions.

5. Dynamics

5.1. Integral Time Scales

As *Davis* [1985*b*] points out, the autocorrelation function of velocity can be a useful diagnostic of the flow. The Eulerian independence time scale

$$T_E^n = \int_0^\infty A^n(t')dt' \qquad (5)$$

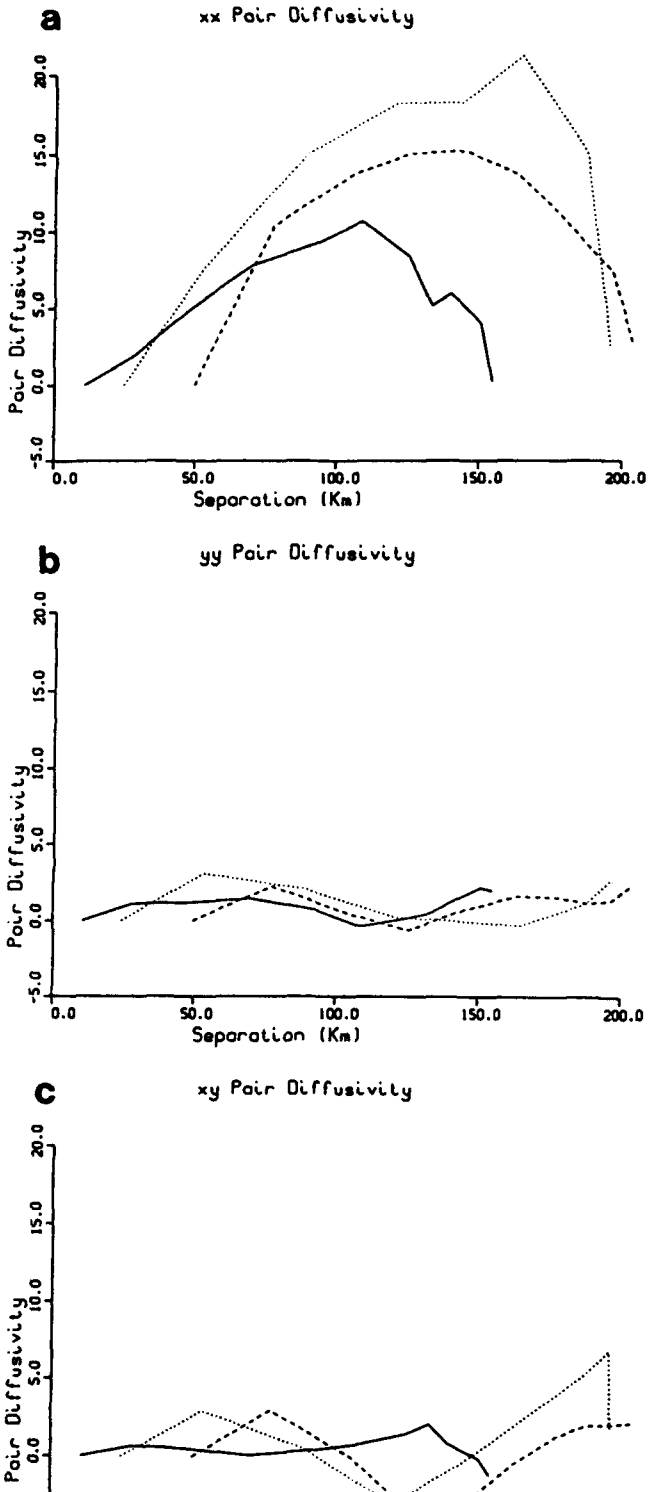

Fig. 9. Pair diffusivities divided by $10^7 cm^2\ s^{-1}$. Initial separation bins can be distinguished by where the curves have $\alpha = 0$. (*a*) Onshore-offshore (xx) component. (*b*) Alongshore (yy) component. (*c*) Off-diagonal (xy) component.

(where A^n is the autocorrelation function of the n component of velocity) is a measure of the typical time scale of velocity changes for an observer located at a fixed point. The analogous Lagrangian time scale

$$T_L^n = \int_0^\infty L^{nn}(t')dt' \tag{6}$$

is a measure of how quickly the velocity changes for a particle being advected through the flow field. A highly nonlinear flow field dominated by semipermanent flow features will likely have $T_L \ll T_E$, whereas a flow field dominated by linear dynamics (flow speeds much less than typical "wave" speeds) will generally have $T_L \cong T_E$ [*Davis*, 1985*b*].

In order to make such a comparison for the coastal transition zone data base, the Eulerian time scale was estimated from the current meter data obtained at depths of 145–200 m (data described by *Stabeno and Smith* [1987]; see also Figure 1). The moored current meters give a typical analogous (one-sided) value of 12 days. This value should be used with caution, however, since the measurements are from a depth range which is much deeper than the near-surface boundary layer (see section 3). Indeed, the current meter velocity fluctuations are a good deal weaker than the surface currents (typically a factor of 4–5). One might expect that near-surface velocity measurements would yield somewhat shorter time scales due to the presence of directly wind-driven flows, but estimates of momentum balances given below suggest that this component of flow may not be large. Thus the 145–200 m current meter estimates may well be reasonable for comparison.

The Lagrangian time scales were estimated by calculating, for all drifters originating in a given box, the Lagrangian autocorrelation function by (3). All calculations were carried out in the same rotated coordinate system as was used for the diffusivity calculations. Given the short time scales involved, all drifters were treated as newly launched 10 days after their *first* appearance, leading to a greater number of degrees of freedom. In many cases, the integral (equation (6)) did not converge even after integrating over 50 days, so the integration was instead truncated at the time of the first zero crossing of the autocorrelation function.

The results of the calculations (Table 1) yield Lagrangian time scales shorter than the Eulerian time scale (12 days), and often much shorter. Thus the hypothesis of fundamentally nonlinear dynamics appears to be validated, at least in the north where current meter data are available. Notice, however, that the idea of nonlinear dynamics does not mean that the nonlinear terms in the momentum equation need to be large. The result means only that such terms must be important relative to the other ageostrophic terms.

5.2. Momentum Balances

It is possible to use the drifter data to estimate the terms in the upper ocean momentum budget. Specifically, we write the horizontal momentum equations as

$$\frac{d\vec{v}}{dt} + f\hat{\vec{k}} \times \vec{v} + \frac{1}{\rho}\nabla p - \frac{1}{\rho}\frac{\partial \vec{\tau}}{\partial z} = 0 \tag{7}$$

where small-scale horizontal turbulent mixing has been neglected. The total derivative is

$$\frac{d}{dt} = \frac{\partial}{\partial t} + u\frac{\partial}{\partial x} + v\frac{\partial}{\partial y} + w\frac{\partial}{\partial z}, \tag{8}$$

where f is the Coriolis parameter, $\hat{\vec{k}}$ is the vertical unit vector, ρ is the density of water, and $\vec{\tau}$ is the vertical component of turbulent stress. If a slablike mixed layer is

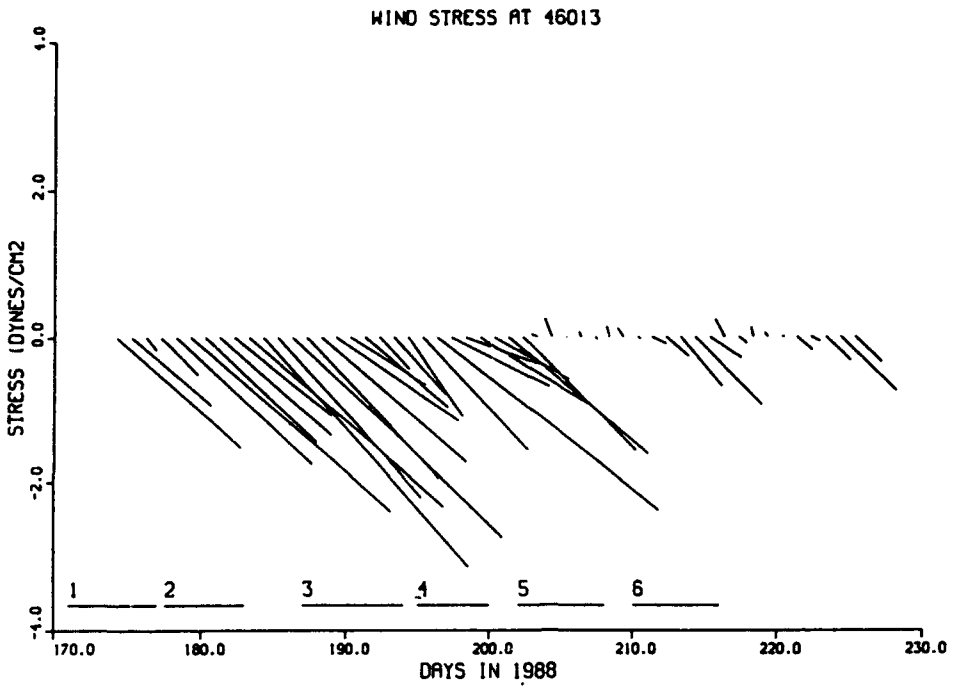

Fig. 10. Wind stress at buoy 46013. North is upward. For reference, July 1 is day 183. Horizontal lines represent the times of hydrographic surveys.

assumed [e.g., *Davis et al.*, 1981], then the vertical gradient of turbulent stress in the mixed layer can be stated as

$$\frac{\partial \vec{\tau}}{\partial z} = h^{-1}\vec{\tau}_0, \tag{9}$$

where h is the mixed layer depth and $\vec{\tau}_0$ is the wind stress applied at the ocean's surface.

Using the drifter data, it is straightforward to estimate the Coriolis force term in (7). Further, the total derivative of velocity is also straightforward to estimate, except that the drifter can not account for the vertical derivative term in (8). The problem then is to estimate the pressure gradient and the mixed layer depth. The approach taken was to consider only those drifters in or near the hydrographic sampling grid (Figure 1) during the time when a particular hydrographic survey was made, typically a period of 6–8 days. Then, during this time, the first two terms in (7) were regressed against the surface wind stress, so that the regression coefficient a could be identified with $(\rho h)^{-1}$. There were four hydrographic surveys during which there were sufficient drifters to carry out this calculation (surveys 3–6). The first three occurred during fairly strong winds, and the last during weak winds (Figure 10). In only one case was a reasonable value of h obtained: map 3, where $h = 26$ m but the x correlation is only 0.17. In all other cases, either a negative or large $O(\geq 80$ m) positive value was obtained for h, in contrast to observed mixed layer depths of $O(20$ m). Finally, the pressure gradient was calculated as the residual of (7) and all results were averaged into 0.5° by 0.5° (latitude by longitude) bins to clarify presentation.

Typical results of a calculation are shown in Figure 11, representing survey 3 on days 187–194 (July 6–13), 1988. The Coriolis (arrow) and acceleration (short stub) terms are compared in Figure 11*a*, while the stress gradient and Coriolis terms are compared in Figure 11*b*. Clearly, the Coriolis term dominates, suggesting a nearly geostrophic balance. The drifter estimate of pressure gradients (dashed arrow) is compared to the pressure gradient based on 0/499 dbar dynamic height in Figure 11*c*. There is a qualitative agreement between the two fields, but it is not very good. The momentum balance results from the three other surveys yielded comparable results.

The poor results of the regression approach should not be surprising. For a velocity within the filament of 50 cm s^{-1}, a Coriolis term of $O(5 \times 10^{-3}$ cm $s^{-2})$ would be anticipated. For a typical wind stress of 1 dyn cm^{-2} and mixed layer depth of 20 m, a typical Ekman velocity would be about 5 cm s^{-1} and the stress gradient term in (7) would be $O(0.5 \times 10^{-3}$ cm $s^{-2})$, small enough to play only a secondary effect relative to the dominating geostrophic balance, and making the regression approach difficult. The poor agreement between the two pressure gradient estimates could have two causes: (1) errors in computing the momentum balance from drifters (including the fact that the drifters are not perfect Lagrangian instruments), and (2) 499 dbar not being the correct level of no motion for the flow field. The moored current results of *Stabeno and Smith* [1987] suggest that a correct level of no motion in this area would lie at a depth of 1000 dbar or greater and that errors associated with the 494-dbar reference level would be 0.0003–0.0012 cm^2 s^{-1}, too small to account for all of the discrepancy in Figure 11*b*, but still limiting our ability to assess the quality of the momentum balance estimates from comparisons.

Nonetheless, some conclusions can be drawn from the momentum balance calculation. First, the lowest-order momentum balance must be geostrophic. This finding is consistent with the validity of quasigeostrophic dynamics. At the next order, Ekman transport and other ageostrophic effects probably enter. It is not possible to say directly whether the total time derivative is dominated by local or advective changes. Results of the time scale calculations (section 5.1)

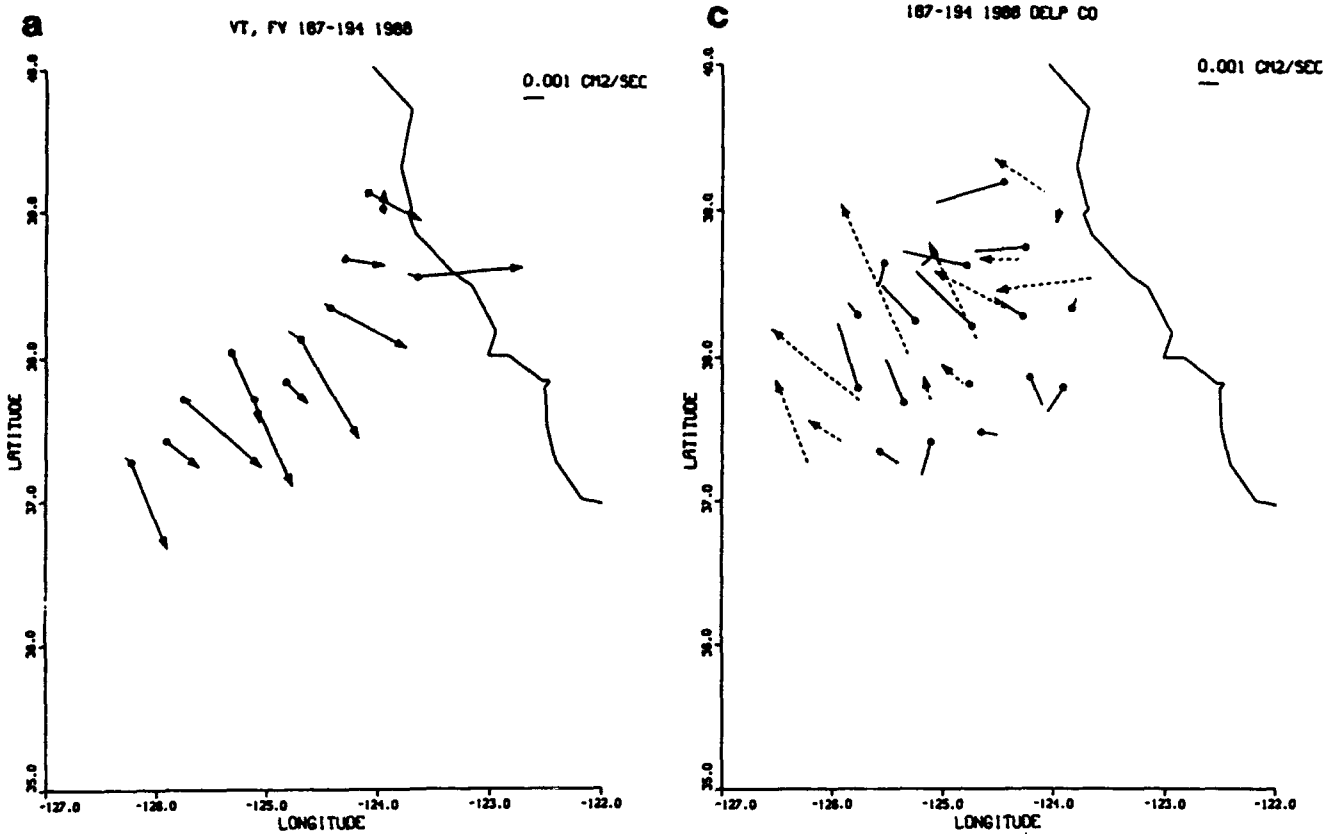

Fig. 11. Results of momentum balance calculations for days 188–195, 1988. (*a*) Coriolis (with arrowhead) and acceleration (without arrowhead) terms. Locations are given by dots. (*b*) Coriolis (with arrowhead) and stress gradient (without arrowhead) terms. (*c*) Comparison pressure gradients computed from drifters (dashed arrows) and from 0/499 dbar dynamic height (solid lines).

Fig. 11. (continued)

suggest, however, that the nonlinear terms must be important.

6. Relation of Near-Surface Flow to Fronts

Very often, filaments have fronts along both their northern and southern sides. Further, there is some evidence that convergence and subduction could be occurring, at least at the southern front [*Flament et al.*, 1985]. It thus seems reasonable to attempt to use the drifter data to look for evidence of such convergence.

The approach used is straightforward. Frontal locations are determined subjectively by using NOAA AVHRR satellite thermal imagery for 1988 only. These are overplotted with drifter positions, so that the shortest distance of a given drifter from both the southern side (η) and northern side (ζ) fronts can be determined. Note that this approach does not depend upon absolute surface temperatures, but rather only on the distance from fronts. Such features should not, over short time scales (days), depend greatly on surface heat fluxes. Most drifters were deployed within the cold waters at the nearshore end of the Point Arena filament. Those that were initially not between the fronts are dropped from the calculation. Histograms of the distance of drifters from the front versus time since launch were then computed (summarized as means and standard deviations in Figure 12). As the drifters proceed offshore in the filament, they draw closer to the south side front, i.e., η decreases. The average distance to the north side front ζ remains roughly constant at about 15 km. This is consistent with the filament narrowing with distance offshore as is typically seen in satellite imagery. These results are also consistent with

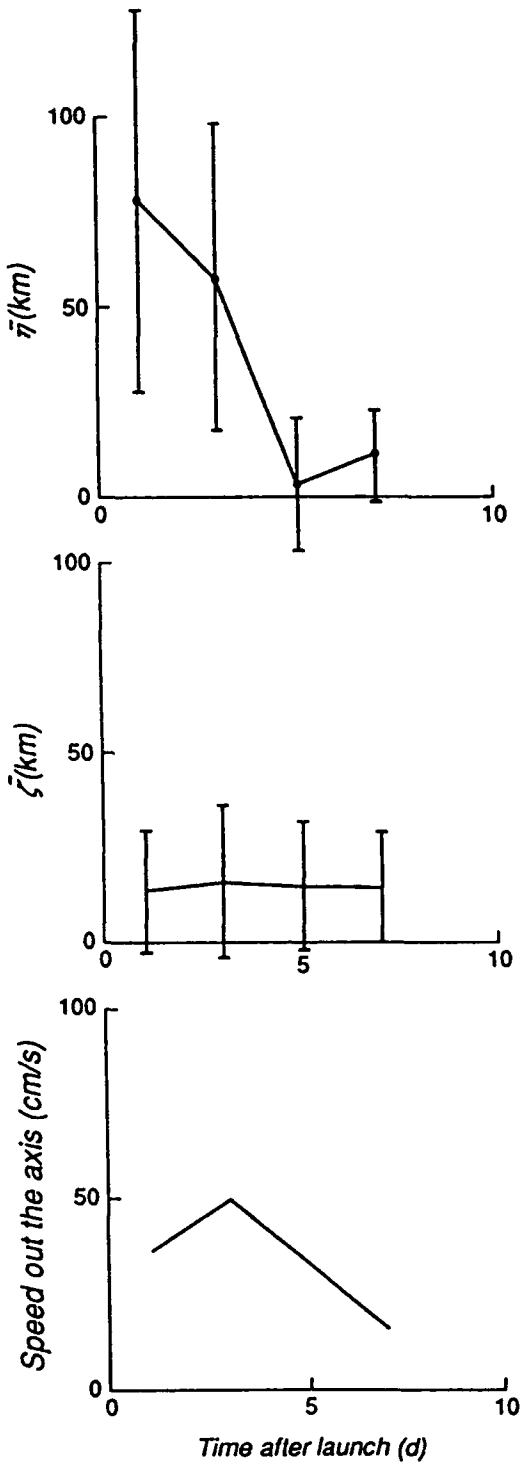

Fig. 12. (*a*) Average distance of drifters from the south side front (η) versus time since launch. Vertical bars represent ± 1 standard deviation. (*b*) Average and standard deviation of drifter distance from the north side front (ζ). (*c*) Average velocity out the filament axis versus time from launch.

convergence on the south side of the filament, but they do not mean that downwelling (subduction) is occurring. For example, the offshore flow in tne filament could simply be accelerating to compensate for the horizontal constriction.

The acceleration hypothesis was tested by computing the average velocity as a function of time for all of the drifters used above. The result (Figure 12) shows that initially the drifters did accelerate but that they slowed down by day 5 from launch. Thus even though the filament becomes narrower, the flow along its axis decelerates, implying downwelling. Most likely, this downwelling occurs at or near the southern side front, since the drifters tend to converge on it (Figure 12). It is straightforward to compute a volume balance for the flow over the upper 15 m of the water column (assuming no flow through the filament edges) to arrive at a downwelling rate of 12 m d^{-1} in the section within the filament 3 to 5 days after deployment (100–170 km from deployment). This rate of sinking is roughly consistent with the 20 m d^{-1} estimate based on biological and chemical tracers [*Kadko et al.*, this issue].

The drifter-based sinking velocity estimate is not very precise. It involves many assumptions, including that no flow crosses the edge of a filament. Further, errors are likely to be introduced by the unavailability of satellite data during cloudy periods, which lasted up to 5 days. Thus, the results need to be taken with caution. This is especially so because Swenson et al. (1990) concluded that downwelling takes place on the northern (not southern) edge of the filament. While their result does not directly call into question our estimate of vertical velocity, it does serve as a caution about the idea that downwelling tends to occur preferentially along the southern side of the filament.

7. CONCLUSIONS

The CTZ drifter results strongly suggest that the California Current between 30° and 40°N has a meandering, jetlike current core. Some of the structure in the current (e.g., the eastward flow near 36°N) appears to be reproducible from 1987 to 1988, although the fairly featureless mean patterns south of 34°N suggest that the core's position varies fairly randomly in that area. The magnitude of the core velocity, the mean velocity and the eddy kinetic energy all tend to decrease toward the south, especially south of about 33°N.

Although the lowest-order momentum balance for the near-surface currents is geostrophic, the governing, higher-order dynamics are more complex. Specifically, the disparity between Eulerian and Lagrangian current time scales suggests that nonlinear effects are quite important. This finding is consistent with the interpretation of the California Current system as being hydrodynamically unstable, e.g., *Ikeda and Emery* [1984] and *Haidvogel et al.* [this issue].

Accompanying the nonlinearity of the flow is a tendency for rapid particle dispersion. The values for both the single point and pair dispersions are substantially larger than those estimated by *Davis* [1985*b*] for an area closer to shore near 38.5°N. *Davis* [1985*b*] also noted that dispersion tended to be isotropic by 50 km from shore, while alongshore dispersion dominated close to the coast. Our results, which represent the region greater than 50 km from shore, show a strong tendency for dominance by the onshore-offshore component of dispersion. This is the opposite sense of anisotropy to that found by *Davis* [1985*b*]. Presumably this difference is related to the coastal inhibition of onshore flow over the shelf, and to the dominance of meandering jet patterns offshore.

The flow field offshore is sufficiently inhomogeneous as to limit Taylor's hypothesis to only order of magnitude validity. This inhomogeneity is also reflected in the substantial spatial variations in kinetic energy and eddy dispersion co-

efficients. This inhomogeneity is roughly consistent with sea level variability estimated with Geosat [*Flament et al.*, 1989].

It now seems very likely that subduction occurs in filaments off northern California, based on chemical and hydrographic tracers [*Kadko et al.*, this issue]. The results of the CTZ drifter study suggest that much of this occurs more than 100 km offshore, and at an area-averaged rate within the filament of $O(10\ \mathrm{m\ d^{-1}})$. Apparently the cold, dense water of the filament core eventually has to sink below the warmer ambient water. By the time the meander causing the filament reverses back toward shore, the cold surface signature is thus greatly reduced. This would account for why satellite temperature and color imagery only tend to "see" flow proceeding offshore.

Acknowledgments. This work was supported by the Office of Naval Research (ONR) through the Coastal Sciences section (code 1122CS).

REFERENCES

Davis, R. E., Drifter observations of coastal surface currents during CODE: The method and descriptive view, *J. Geophys. Res.*, *90*, 4741–4755, 1985*a*.

Davis, R. E., Drifter observations of coastal surface currents during CODE: The statistical and dynamical views, *J. Geophys. Res.*, *90*, 4756–4772, 1985*b*.

Davis, R. E., R. A. DeSzoeke, and P. P. Niiler, Variability in the upper ocean during MILE, II, Modeling the mixed-layer response, *Deep Sea Res.*, *28*, 1453–1476, 1981.

Flament, P., L. Armi, and L. Washburn, The evolving structure of an upwelling filament, *J. Geophys. Res.*, *90*, 11,765–11,778, 11,835–11,836, 1985.

Flament, P., P. M. Kosro, and A. Huyer, Mesoscale variability off California as seen by the Geosat altimeter, in *Proceedings of the International Geoscience and Remote Sensing Symposium, Vancouver, 1989, vol. 2*, I.E.E.E., New York, 1063–1068, 1989.

Fleischbein, J., R. E. Schramm, A. Huyer, P. M. Kosro, T. Cowles, K. Krefft, and C. Paulson, CTD observations in the coastal transition zone off northern California from R/V *Wecoma*, July to August 1988, *Data Rep.144*, *Ref. 89-1*, 242 pp, Oreg. State Univ., Corvallis, 1989.

Haidvogel, D. B., A. Beckmann, and K. S. Hedström, Dynamical simulations of filament formation and evolution in the coastal transition zone. *J. Geophys. Res.*, this issue.

Hickey, B. M., The California Current system — Hypothesis and facts, *Prog. Oceanogr.*, *8*, 191–279, 1979.

Huyer, A., P. M. Kosro, J. Fleischbein, S. R. Ramp, T. Stanton, L. Washburn, F. P. Chavez, T. J. Cowles, S. D. Pierce, and R. L. Smith, Currents and water masses of the coastal transition zone off northern California, June to August 1988, *J. Geophys. Res.*, this issue.

Ikeda, M., and W. J. Emery, Satellite observations and modeling of meanders in the California Current system off Oregon and northern California, *J. Phys. Oceanogr.*, *14*, 1434–1450, 1984.

Kadko, D. C., L. Washburn, and B. Jones, Evidence of subduction within cold filaments of the northern California coastal transition zone, *J. Geophys. Res.*, this issue.

Kelly, K. A., and R. E. Davis, An analysis of errors in sea surface temperature in a series of infrared images from NOAA 6, *J. Geophys. Res.*, *91*, 2633–2644, 1986.

Kosro, P. M., A. Huyer, S. R. Ramp, R. L. Smith, F. P. Chavez, T. J. Cowles, M. R. Abbott, P. T. Strub, R. T. Barber, P. Jessen, and L. F. Small, The structure of the transition zone between coastal waters and the open ocean off northern California, winter and spring 1987, *J. Geophys. Res.*, this issue.

Krauss, W., and C. W. Böning, Lagrangian properties of eddy fields in the northern North Atlantic as deduced from satellite-tracked buoys, *J. Mar. Res.*, *45*, 259–291, 1987.

Kundu, P. K., and J. S. Allen, Some three-dimensional characteristics of low-frequency current fluctuations near the Oregon coast, *J. Phys. Oceanogr.*, *6*, 181–199, 1976.

Large, W. G., and S. Pond, Open ocean momentum flux measurements in moderate to strong winds, *J. Phys. Oceanogr.*, *11*, 324–336, 1981.

Niiler, P. P., R. E. Davis, and H. J. White, Water-following characteristics of a mixed layer drifter, *Deep Sea Res.*, *34*, 1867–1881, 1987.

Poulain, P.-M., and P. P. Niiler, Statistical analysis of the surface circulation in the California current system using satellite-tracked drifters, *J. Phys. Oceanogr.*, *19*, 1588–1603, 1989.

Stabeno, P. J., and R. L. Smith, Deep-sea currents off northern California, *J. Geophys. Res.*, *92*, 755–771. 1987.

M. Abbott and A. Huyer, College of Oceanography, Oregon State University, Corvallis, OR 97331.

R. C. Beardsley and K. H. Brink, Woods Hole Oceanographic Institution, Woods Hole, MA 02543.

P. P. Niiler, Scripps Institution of Oceanography, University of California, San Diego, La Jolla, CA 92093.

S. Ramp and T. Stanton, Department of Oceanography, Naval Postgraduate School, Monterey, CA 93943.

D. Stuart, Department of Meteorology, Florida State University, Tallahassee, FL 32306.

(Received June 29, 1990;
accepted October 14, 1990.)